Tunable terahertz wave add-drop filter

LI JIU-SHENG*, YU JIA-PEI, ZHANG LE, HU JIAN-RONG, QIU GUO-HUA
Centre for THz Research, China Jiliang University, Hangzhou 310018, China

We proposed a tunable terahertz wave add-drop filter based on a rectangular defect rod, an elliptical defect rod, and two output line-defect waveguides in square lattice photonic crystal silicon rods. The coupled mode theory and finite-difference time-domain method are employed to analyze the transmission properties of the device. Through merely changing the refractive index of the defect rods, the add-drop operating frequency of the proposed filter can be easily varied from 0.2959 THz to 0.3005 THz. The adding and dropping efficiency of the proposed structure are close to 93.6% and 99.0%, respectively.

(Received June 6, 2017; accepted April 5, 2018)

Keywords: Terahertz wave, Terahertz add-drop filter, Photonic crystal

1. Introduction

Photonic crystals, artificial wavelength-scale structures with periodic dielectric arrays, have attracted a great deal of research attentions due to their photonic band-gap and strong photon confinement effect, which cannot be obtained in nature materials. Over the last few decades, a variety of functional devices based on photonic crystal have been demonstrated to manipulate electromagnetic waves in visible light spectrum and microwave region [1-5]. Being very weak response to the terahertz wave, many natural materials are hard to construct terahertz devices. Due to the unique properties, photonic crystal provides a sufficient way to realize the terahertz wave functional devices. In particular, with rapidly development of terahertz wave science and technology, terahertz wave manipulation devices will be greater in demand than ever. More recent, some researchers have demonstrated some devices based on photonic crystal in terahertz region, such as filters [6-7], switches [8-9], power dividers [10] and modulators [11-12]. Over the past few years, considerable efforts have been devoted to the development of terahertz manipulated devices for applications in terahertz spectroscopy, medical science, communication, and imaging systems [13-14]. So far, unfortunately, as one of the most important and essential components in constructing a terahertz wavelength division multiplexing system, tunable terahertz add-drop filter has not yet been sufficiently exploited. In order to convenient construct a terahertz wavelength division multiplexing system, however, dynamically tunable, compact, responding fast is still required for terahertz add-drop filter. A convenient and effective method to achieve fast-tunable function and structural simplicity for cost reduction as well as extremely high add-drop efficiency should be more widely explored. It is well known that, by introducing the defects in the photonic crystal, terahertz wave components can be realized. A photonic crystal hybrid structure with resonant coupling between micro-cavity modes produced by point defects and waveguide modes created by line defects seems to be one promising approach to obtain the high performance terahertz add-drop filter. To facilitate device design based on this novel paradigm, the mechanisms by which resonant coupling modes between point defect rod and line defect waveguide in photonic crystals, remains to be clarified.

In this letter, we investigate a new type of tunable terahertz wave add-drop filter based on the two dimensional square lattice photonic crystals with two defect waveguides (One is bus waveguide, another is drop waveguide), a rectangular defect rod, and an elliptical defect rod. Two-dimensional finite-difference time-domain method with perfectly matched layers has been used to calculate the transmission performance of the presented device. Adding efficiency of 93.6% and dropping efficiency up to 99.0% can be achieved in terahertz wave communication window. Through altering the refractive index of the defect rods, the add-drop frequency of the proposed device can be easily changed from 0.2959THz to 0.3005THz.

2. Theory analysis

In this letter, the configuration used for the terahertz add-drop filter is based on two-dimensional square lattice photonic crystal of high resistivity Si rods with radius r=0.22a (where a is the lattice constant) in the air host. Here, the loss of the high resistivity silicon is very weak in the terahertz region and its refractive index is 3.45. Sketch map of the terahertz add-drop filter consists of a rectangular defect rod, an elliptical defect rod, and two

line-defect waveguides. Fig. 1 illustrates the presented device structure and its three ports labeled as A, B, and C. In the figure, the red rods (rectangular rod and elliptical rod) are made of polystyrene (refractive index n=1.59), whose refractive index can be changed as the applied external pump laser intensity change [11]. When the pump laser powers are of 6.33, 6.45, 6.56 MW/cm^2, the refractive index of polystyrene becomes as 1.62, 1.65, 1.68, respectively. The length of the square rod is 0.47a, while the major axis of the ellipse rod is 1.344a and the minor axis of the ellipse rod is 0.27a. The theoretical modeling of the terahertz add-drop filter is illustrated in Fig. 2. The rectangle and the elliptical polystyrene rods forms two point-defect cavities, as shown in both Fig. 1 and Fig. 2, which can only support one guide-mode in the frequency range of interest.

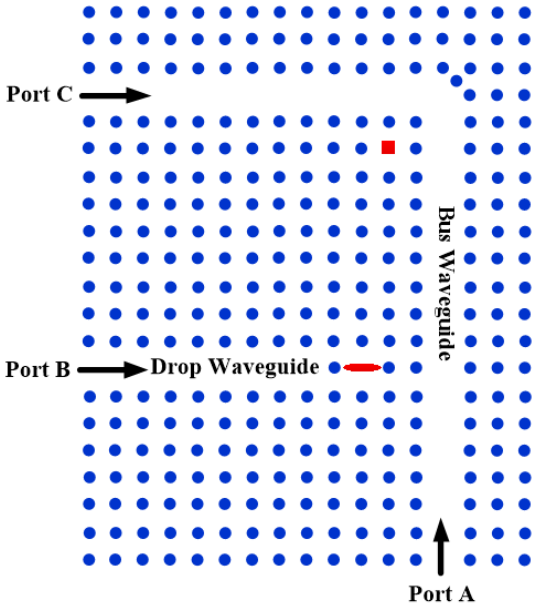

Fig. 1. Configuration of the proposed terahertz add-drop filter

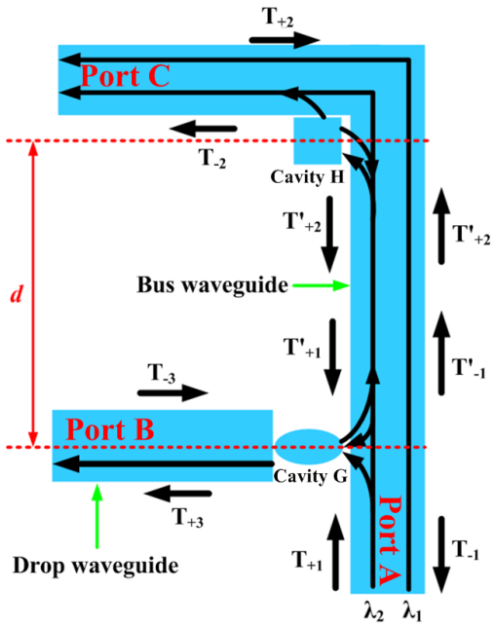

Fig. 2. Theoretical modeling of the proposed terahertz add-drop filter

Fig. 2 shows the amplitudes of the incoming (outgoing) waves in the line-defect waveguides denoted by $T_{\pm i}$ and $T'_{\pm i}$. Meanwhile, the time evolution of the amplitudes of the cavity G and H are denoted by g and h, respectively. According to the coupled-mode theory [15-17], the amplitudes of the incoming (outgoing) waves in the add-drop filter can be described by

$$\frac{dg}{dt}=\left(j\omega_g-\frac{\omega_g}{Q_g}-\frac{\omega_g}{2Q_1}-\frac{\omega_g}{2Q_2}\right)g+e^{j\theta_1}\sqrt{\frac{\omega_g}{2Q_1}}T_{+1}+e^{j\theta_1}\sqrt{\frac{\omega_g}{2Q_1}}T'_{+1}+e^{j\theta_2}\sqrt{\frac{\omega_g}{Q_2}}T_{+3} \tag{1}$$

$$\frac{dh}{dt}=\left(j\omega_h-\frac{\omega_h}{Q_h}-\frac{\omega_h}{2Q_3}\right)h+e^{j\theta_3}\sqrt{\frac{\omega_h}{2Q_3}}T_{+2}+e^{j\theta_3}\sqrt{\frac{\omega_h}{2Q_3}}T'_{+2} \tag{2}$$

where $T_{-2}=T'_{+2}-e^{-j\theta_3}\sqrt{\frac{\omega_h}{2Q_3}}h$, $T'_{-2}=T_{+2}-e^{-j\theta_3}\sqrt{\frac{\omega_h}{2Q_3}}h$,

$$T'_{+2}=T'_{-1}e^{-j\beta d},\quad T'_{+1}=T'_{-2}e^{-j\beta d},\quad T'_{-1}=T_{+1}-e^{-j\theta_1}\sqrt{\frac{\omega_g}{2Q_1}}g,$$

$$T_{-1}=T'_{+1}-e^{-j\theta_1}\sqrt{\frac{\omega_g}{2Q_1}}g,\quad T_{-3}=-T_{+3}+e^{-j\theta_2}\sqrt{\frac{\omega_g}{Q_2}}g,\quad \omega_g$$

and ω_h are the resonant frequencies of the cavity G and H, respectively. Q_g and Q_h are the quality factors due to intrinsic loss of the cavity G and H, respectively. Q_1=$\omega_g\tau_1$/2 and Q_3=$\omega_h\tau_3$/2 is the decay rate into the bus waveguide of cavity G and H at τ_1 and τ_3, respectively. Q_2=$\omega_g\tau_2$/2 is the decay rate into the drop waveguide of cavity G at τ_2. θ_1 and θ_2 are the phases of the coupling coefficients between the cavity G and the bus/drop waveguide, respectively, θ_3 is the phase of coupling coefficient between the cavity H and the bus waveguide, β is the propagation constant of the bus waveguide, and d is the distance between the two point-defect cavities. When the wave is lunched in the input port (i.e. T_{+2}=0, T_{+3}=0), by solving Eqs.(1) to (2), T'_{+1} can be given by

$$T'_{+1} = -\frac{1}{2Q_3\left(j\left(\frac{\omega}{\omega_h}-1\right)+\frac{1}{2Q_b}+\frac{1}{2Q_3}\right)} e^{-j2\beta d}\left(T_{+1} - e^{-j\theta_1}\sqrt{\frac{\omega_g}{2Q_1}}g\right) \tag{3}$$

We know $\phi=2\beta d$, substituting Eq.(10) into Eq.(1), the g can be calculated by

$$g = \frac{e^{-j\theta_1}\sqrt{\frac{\omega_g}{2Q_1}}\left[1-m\left(\cos\varphi - j\sin\varphi\right)\right]T_{+1}}{j\omega_g\left(\frac{\omega}{\omega_g}-1+\frac{m}{2Q_1}\sin\varphi\right)+\frac{\omega_g}{Q_g}+\frac{\omega_g}{2Q_2}+\frac{\omega_g}{2Q_1}\left(1-m\cos\varphi\right)} \tag{4}$$

$$m = \frac{1}{2Q_3\left(j\left(\frac{\omega}{\omega_h}-1\right)+\frac{1}{Q_h}+\frac{1}{2Q_3}\right)} \tag{5}$$

Substituting Eq.(3) in Eq.(1) to Eq.(2), we can obtain the transmission through the drop waveguide as follow

$$T = \frac{T_{-3}}{T_{+1}} = \frac{e^{-j\theta_1-j\theta_2}\sqrt{\frac{1}{Q_1Q_2}}\left[1-m\left(\cos\varphi - j\sin\varphi\right)\right]}{j\left(\frac{\omega}{\omega_g}-1+\frac{m}{2Q_1}\sin\varphi\right)+\frac{1}{Q_g}+\frac{1}{2Q_2}+\frac{1}{2Q_1}\left(1-m\cos\varphi\right)} \tag{6}$$

When $Q_g >> Q_1$, $Q_h >> Q_3$, $\omega=\omega_g=\omega_h$, and $k=Q_1/Q_2$, substituting Eq.(4) to Eq.(6), the drop efficiency η can be denoted by

$$\eta = |T|^2 = \frac{4k\left(1-\cos\varphi\right)}{k^2+2k\left(1-\cos\varphi\right)+2\left(1-\cos\varphi\right)} \tag{7}$$

From the Eq.(7), one sees that the drop efficiency achieves the maximum value when $k=2$ and $\phi=(2n+1)\pi$, which can be used to guide our design of the proposed configuration.

3. Results and discussion

By using plane wave expansion method, we can calculate the band-gap diagram for the perfect photonic crystal, as shown in Fig. 3. In this structure, one photonic band-gap changes from 0.2682(a/λ) to 0.3920(a/λ) and another photonic band-gap is ranging from 0.5194(a/λ) to 0.5464(a/λ). In this letter, the constant lattice is set to be a=330μm. Fig. 4 shows the dispersion curve of the bus and the drop waveguides, in which a normalized single-mode frequency from 0.295(a/λ) to 0.391(a/λ) is supported. According to the analysis as above in section 2, when $Q_1/Q_2=2$, the distance between the two point-defect cavities is of $d=8a$. In order to meet the $\phi=2\beta d=(2n+1)\pi$ and achieve the maximum drop efficiency, we can obtain $\phi=5\pi$. Correspondingly, the four resonance frequencies of the presented device are 0.3306(a/λ), 0.3288(a/λ), 0.3273(a/λ), and 0.3255(a/λ) when the refractive index of polystyrene are n=1.59, n=1.62, n=1.65 and n=1.68, respectively. A terahertz wave pulse, covering the frequency of 0.3306(a/λ), 0.3288(a/λ), 0.3273(a/λ), and 0.3255(a/λ) are launched at the input port A. Power monitors were placed at the ports B and C to collect the transmitted spectral power density after Fourier-transformation, which are normalized to the incident terahertz wave spectral power density from input port A.

The terahertz transmission characteristics of the add-drop filter are simulated using the commercial finite-difference time-domain method software Rsoft with perfectly matched layers as absorbing boundaries. Figs. 5(a) and 5(b) show the normalized transmission spectra of the port B and port C for different refractive index of defect rods n=1.59, n=1.62, n=1.65 and n=1.68, respectively. From the figures, it can be noted that the resonance frequencies are tunable by means of a localized change the defect rods refractive index. A red shift in resonant frequency is observed as the refractive index of the defect rods increases, while the full width at half maximum is near to 2.0GHz and the transmission efficiency is over 95% (see Fig. 5(a)). This achieves a tunable terahertz wave add-drop filter. Furthermore, it can also be observed that the spectral selectivity is larger than 95.6% drop efficiency at the resonant frequency. From the Fig. 5(b), when the drop efficiency of the port B achieves the maximum value, the transmission amplitude of the port C is close to 0 for different refractive index of the defect rods at frequencies of 0.3005THz, 0.2990THz, 0.2975THz, and 0.2959THz, respectively. The transmission efficiency of port B for different refractive index of defect rods is summarized in Table 1. At last, the steady field distribution is simulated by using finite-difference time-domain method with a continued mono-frequency terahertz wave. The terahertz wave is launched into input waveguide until the field distribution is stable. Snapshots of the steady-state field distributions at port B and C for different refractive index of the defect rods are shown in Figs. 6(a)~6(h). According to Figs. 6(a), 6(c), 6(e), and 6(g), the terahertz wave can propagate from port A to port B while the terahertz source is set as the resonant frequency (i.e. 0.3005THz, 0.2990THz, 0.2975THz, and 0.2959THz) at port A. However, the terahertz wave can not pass through the point-defect rod G when the input terahertz wave is not at the resonant frequency (see the Figs. 6(b), 6(d), 6(f), and 6(h)). Combined with the transmission curves in Fig. 5 and the steady state electric field distribution in Fig. 6, one can see that there has good agreement between theory calculation and simulation results.

According to the Figs. 5 and 6, the tunable drop characteristics of the add-drop filter are simulated. To give comprehensive understanding, a terahertz pulse launched at the port B at frequencies of 0.3306(a/λ), 0.3288(a/λ), 0.3273(a/λ), and 0.3255(a/λ) are used to evaluate the add-drop performance of the filter. Power monitors were

placed at each of the ports A and C to collect the transmitted spectral power density after Fourier-transformation. Fig. 7 depicts the transmission spectra of the defect rods refractive index as n=1.59, n=1.62, n=1.65 and n=1.68. It can be noted that the corresponding resonant frequency can transmit from the port B to port A. However, at this time, the transmission amplitude of the port C is close to 0. The transmission efficiency is larger than 90.4% and is summarized in Table 2. Figs. 8(a)~8(h) show the steady state electric field distributions at frequencies of 0.3306(a/λ), 0.3288(a/λ), 0.3273(a/λ), and 0.3255(a/λ) for different refractive index of the defect rods, respectively. From Figs. 8(a), 8(c), 8(e), and 8(g), one sees that the terahertz wave propagates from port B to port A at the resonant frequency of 0.3005THz, 0.2990THz, 0.2975THz, and 0.2959THz. When the input terahertz wave is not the resonant frequency at port B, the terahertz wave can not propagates from port B to port A, as shown in Figs. 8(b), 8(d), 8(f), and 8(h). With the attractive characteristics described above, the proposed tunable terahertz add-drop filter is a promising candidate for the future terahertz wavelength division multiplexing system.

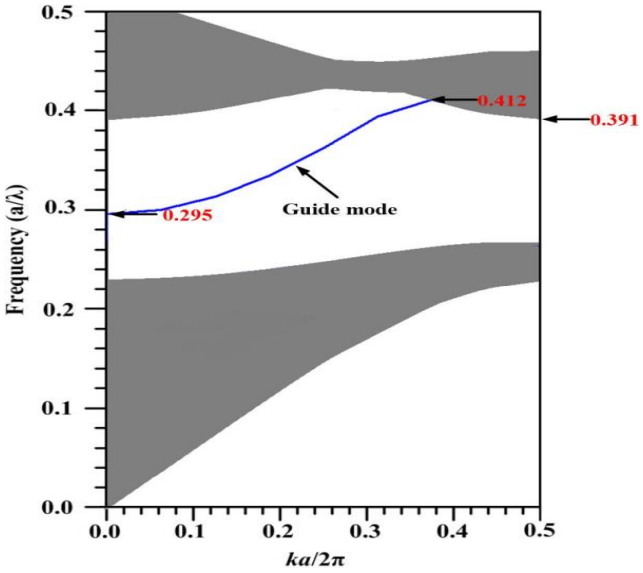

Fig. 4. Dispersion curves for transverse electric mode of the photonic crystals after introducing bus waveguide and drop waveguide

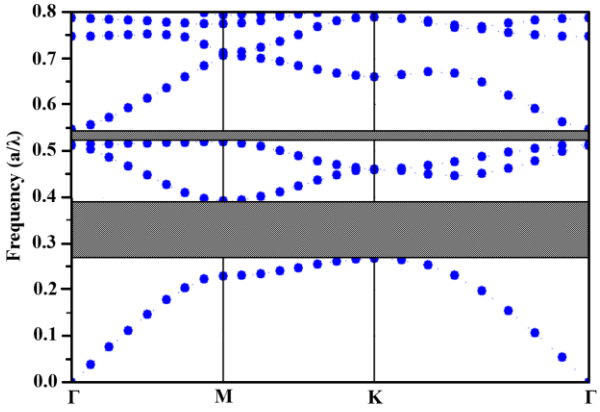

Fig. 3. Band structure diagrams of the photonic crystals structure without defect for transverse electric mode

Table 1. Transmission efficiency of Port B for different refractive index of defect rods

Refractive Index of the defect rods (n)	Central Frequency (THz)	Transmission Efficiency	Full Width at Half Maximum (GHz)
1.59	0.3005	95.6%	2
1.62	0.2990	99.0%	2.25
1.65	0.2975	97.0%	2
1.68	0.2959	96.7%	1.7

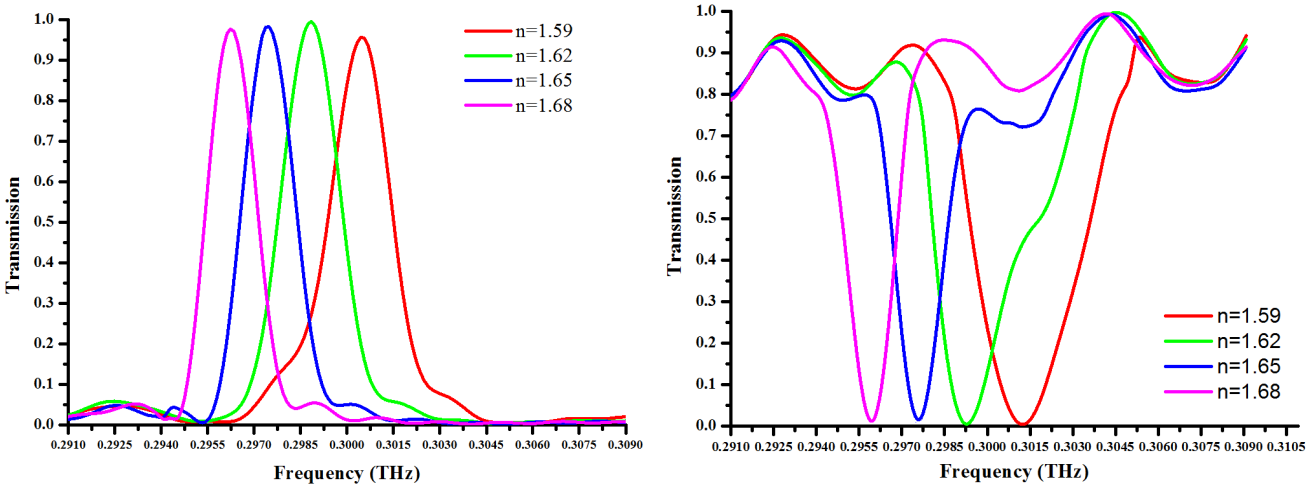

Fig. 5. Transmission spectra of (a) port B, (b) port C for different refractive index of the defect rods

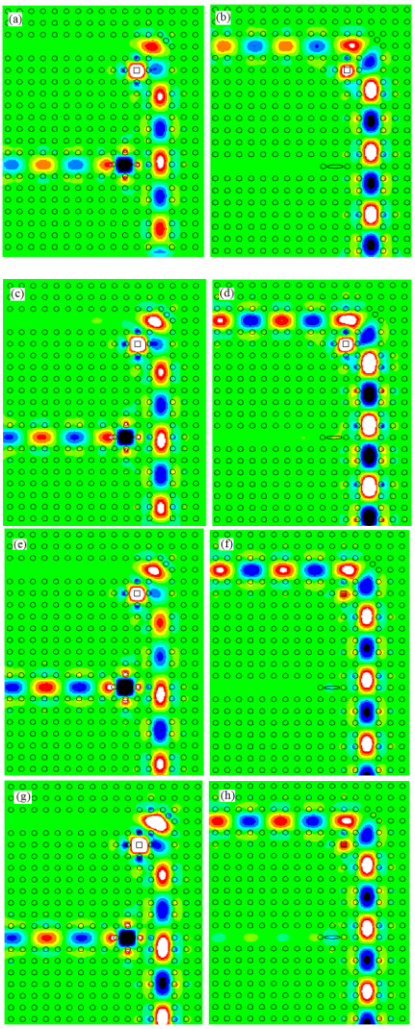

Fig. 6. Steady state electric field distribution at port B and C for different refractive index of the defect rods, (a) n=1.59, f=0.3005THz; (b) n=1.59, f=0.3054THz; (c) n=1.62, f=0.2989THz; (d) n=1.62, f=0.3036THz; (e) n=1.65, f=0.2975THz; (f) n=1.65, f=0.3018THz; (g) n=1.68, f=0.2959THz; (h) n=1.68, f=0.3THz

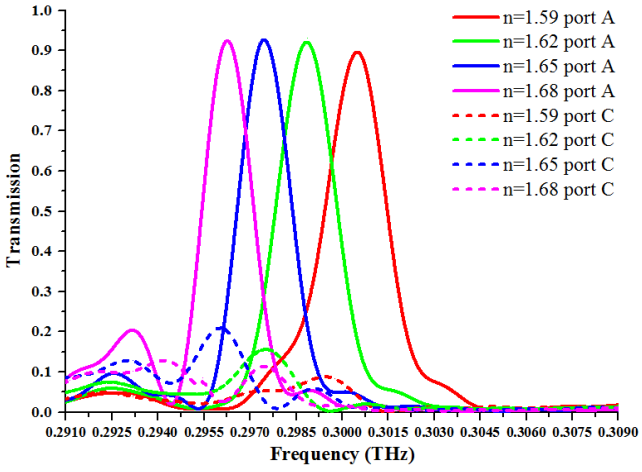

Fig. 7. Transmission spectra of port A and C for different refractive index of defect rods

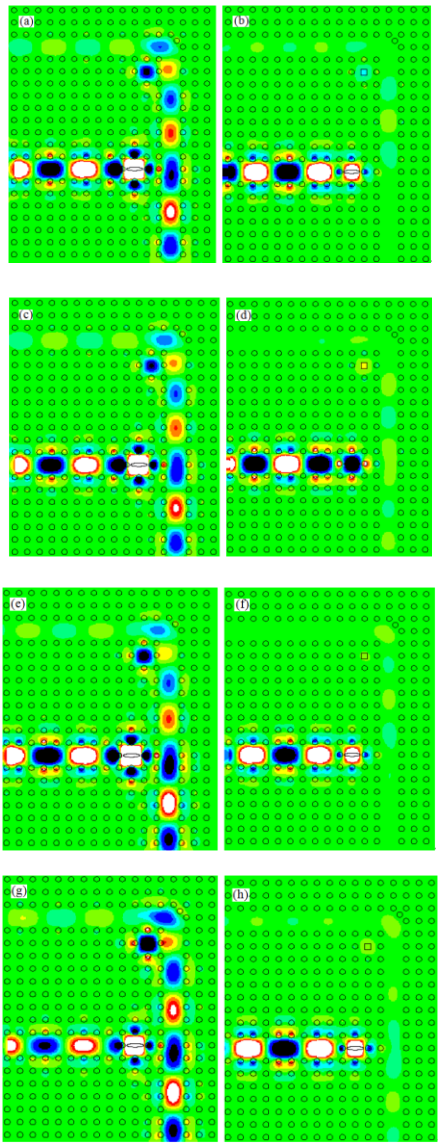

Fig. 8. Steady state electric field distribution at port A and C for different refractive index of defect rods, (a) n=1.59, f=0.3005THz; (b) n=1.59, f=0.3054THz; (c) n=1.62, f=0.2989THz; (d) n=1.62, f=0.3036THz; (e) n=1.65, f=0.2975THz; (f) n=1.65, f=0.3018THz; (g) n=1.68, f=0.2959THz; (h) n=1.68, f=0.3THz

Table 2. Transmission efficiency of Port A for different refractive index of defect rods

Refractive Index of the defect rods (*n*)	Central Frequency (THz)	Transmission Efficiency	Full Width at Half Maximum (GHz)
1.59	0.3005	90.4%	2.5
1.62	0.2990	93.0%	2.3
1.65	0.2975	93.6%	1.8
1.68	0.2959	92.7%	1.7

4. Conclusions

In this study, we designed and simulated a tunable terahertz add-drop filter performances based on the two-dimensional photonic crystal structure with a rectangular defect rod, an elliptical defect rod, and two defect waveguides. The transmission characteristics of the device were demonstrated by using the two-dimensional finite-difference time-domain method and coupled-mode theory. The add-drop frequency from 0.2959 THz to 0.3005 THz can be adjusted by altering the refractive index of the defect rods. Dropped efficiency close to 100% (>99.0%) can be achieved in the add-drop filter at 0.299 THz. The total size of the device is $16a \times 20a$. Therefore, the tunable add-drop filter may be potentially applied in the terahertz wavelength division multiplexing devices.

Acknowledgments

This research was supported by the National Natural Science Foundation of China No. 61379024.

References

[1] B. Ellis, M. Mayer, G. Shambat, T. Sarmiento, J. Harris, E. Haller, J. Vučković, Nat. Photon. **5**, 297 (2011).
[2] Z. Qiang, W. Zhou, R. Soref, Optics Express **15**, 1823 (2007).
[3] B. Ellis, T. Sarmiento, M. Mayer, B. Zhang, J. Harris, E. Haller, J. Vuckovic, Appl. Phys. Lett. **96**, 181103 (2010).
[4] Y. Akahane, T. Asano, B. Song, S. Noda, Nature **425**, 944 (2003).
[5] M. Birjandi, A. Tavousi, M. Ghadrdan, Photonics and Nanostr.-Fundamentals and Appl. **21**, 44 (2016).
[6] J. Li, Opt. Commun. **283**, 2647 (2010).
[7] H. Zhang, P. Guo, P. Chen, S. Chang, J. Yuan, J. Opt. Soc. Am. B **26**(1), 101 (2009).
[8] M. Javan, N. Granpayeh, J. Electromagnetic Waves and Applications **23**, 203 (2009).
[9] Y. Kim, S. Lin, H. Wu, R. Pan, J. Applied Physics **109**, 123111 (2011).
[10] S. Li, H. Zhang, Q. Wen, Y. Song, W. Ling, Y. Li, Applied Physics B **95**(4), 745 (2009).
[11] J. Li, Opt. Commun. **296**, 137 (2013).
[12] L. Fekete, F. Kadlec, H. Němec, P. Kužel, Optics Express **15**, 8898 (2007).
[13] Y. Chiang, C. Yang, Y. Yang, C. Pan, T. Yen, Appl. Phys. Lett. **99**(19), 191909 (2011).
[14] X. Zhou, X. Yin, T. Zhang, L. Chen, X. Li, Optics Express **23**(9), 11657 (2015).
[15] S. Kim, I. Park, H. Lim, Optics Express **12**(22), 5518 (2004).
[16] H. Ren, C. Jiang, W. Hu, M. Gao, J. Wang, Optics Express **14**(6), 2446 (2006).
[17] Y. Xu, Y. Li, R. Lee, A. Yariv, Phys. Rev. E **62**, 7389 (2000).

*Corresponding author: forever-li@126.com